Monthly Notices
of the
ROYAL ASTRONOMICAL SOCIETY

MNRAS **468,** 2822–2835 (2017)
Advance Access publication 2017 March 9

doi:10.1093/mnras/stx585

# *NuSTAR* and *XMM–Newton* observations of the Arches cluster in 2015: fading hard X-ray emission from the molecular cloud

Roman Krivonos,[1⋆] Maïca Clavel,[2⋆] JaeSub Hong,[3] Kaya Mori,[4] Gabriele Ponti,[5] Juri Poutanen,[6,7] Farid Rahoui,[8,9] John Tomsick[2] and Sergey Tsygankov[6]

[1]*Space Research Institute of the Russian Academy of Sciences, Profsoyuznaya Str. 84/32, 117997 Moscow, Russia*
[2]*Space Sciences Laboratory, University of California, 7 Gauss Way, Berkeley, CA 94720-7450, USA*
[3]*Harvard-Smithsonian Center for Astrophysics, 60 Garden Street, Cambridge, MA 02138, USA*
[4]*Columbia Astrophysics Laboratory, Columbia University, New York, NY 10027, USA*
[5]*Max-Planck-Institut für extraterrestrische Physik, Giessenbachstrasse 1, D-85748 Garching, Germany*
[6]*Tuorla Observatory, Department of Physics and Astronomy, University of Turku, Väisäläntie 20, FI-21500 Piikkiö, Finland*
[7]*Nordita, KTH Royal Institute of Technology and Stockholm University, Roslagstullsbacken 23, SE-10691 Stockholm, Sweden*
[8]*European Southern Observatory, Karl-Schwarzschild-Str. 2, D-85748 Garching, Germany*
[9]*Department of Astronomy, Harvard University, 60 Garden Street, Cambridge, MA 02138, USA*

Accepted 2017 March 7. Received 2017 March 3; in original form 2016 December 10

## ABSTRACT

We present results of long *Nuclear Spectroscopic Telescope Array* (*NuSTAR*; 200 ks) and *XMM–Newton* (100 ks) observations of the Arches stellar cluster, a source of bright thermal ($kT \sim 2$ keV) X-rays with prominent Fe XXV K$\alpha$ 6.7 keV line emission and a nearby molecular cloud, characterized by an extended non-thermal hard X-ray continuum and fluorescent Fe K$\alpha$ 6.4 keV line of a neutral or low-ionization state material around the cluster. Our analysis demonstrates that the non-thermal emission of the Arches cloud underwent a dramatic change, with its homogeneous morphology, traced by fluorescent Fe K$\alpha$ line emission, vanishing after 2012, revealing three bright clumps. The declining trend of the cloud emission, if linearly fitted, is consistent with half-life decay time of ∼8 yr. Such strong variations have been observed in several other molecular clouds in the Galactic Centre, including the giant molecular cloud Sgr B2, and point towards a similar propagation of illuminating fronts, presumably induced by the past flaring activity of Sgr A⋆. We also detect a significant drop of the equivalent width of the fluorescent Fe Ka line, which could mean either that the new clumps have a different position along the line of sight or that the contribution of cosmic ray has become more dominant.

**Key words:** ISM: clouds – X-rays: individual: Arches cluster.

## 1 INTRODUCTION

The Arches cluster is a massive star cluster with a core radius of about 9 arcsec (∼0.35 pc at 8 kpc) (Figer et al. 1999), containing more than 160 O-type stars (Figer et al. 2002). It is located in the inner Galactic Centre (GC) region at the projected angular distance of 11 arcmin from Sgr A⋆. *Chandra* observations of the Arches cluster region revealed a complicated picture of the X-ray emission, showing the presence of spatially separated thermal and non-thermal emission components. The thermal emission is thought to originate from multiple collisions between strong winds of massive stars within the stellar cluster (Yusef-Zadeh et al. 2003; Wang, Dong & Lang 2006; Capelli et al. 2011a). Diffuse non-thermal X-ray emission has been detected from a broad region ('clouds') around the cluster (Wang et al. 2006; Tsujimoto, Hyodo & Koyama 2007; Capelli et al. 2011b; Tatischeff, Decourchelle & Maurin 2012; Krivonos et al. 2014). The non-thermal nature of this extended radiation is revealed by its strong fluorescent Fe K$\alpha$ 6.4 keV line emission, presumably coming from material that is neutral or in a low-ionization state.

Two physical mechanisms to produce fluorescent emission in the molecular clouds are generally discussed. The first implies reflection of incoming hard X-rays where K-shell photoionization and the subsequent fluorescence produce a strong Fe K$\alpha$ line with an equivalent width (EW) $\gtrsim$ 1 keV (Markevitch, Sunyaev & Pavlinsky 1993; Sunyaev, Markevitch & Pavlinsky 1993; Koyama et al. 1996; Sunyaev & Churazov 1998). Additionally, the Compton scattering of high-energy photons results in a reflection hump around 20–30 keV. The source of the incoming X-rays might be associated with a nearby X-ray source (e.g. Churazov et al. 1993, 1E 1740.7−2942) or with past activity of Sgr A⋆, as suggested by

⋆ E-mail: krivonos@iki.rssi.ru (RK); maica.clavel@ssl.berkeley.edu (MC)

Sunyaev et al. (1993) to explain the hard X-ray emission of the giant molecular cloud Sgr B2 in the GC region, leading to prediction of the bright 6.4 keV line later confirmed by the observations (Koyama et al. 1996; Sunyaev & Churazov 1998; Murakami et al. 2000; Revnivtsev et al. 2004; Terrier et al. 2010; Zhang et al. 2015). A long outburst from Sgr A$^\star$ lasting more than 10 yr and ending a few hundred years ago could explain the Sgr B2 emission (Koyama et al. 1996; Terrier et al. 2010). The hypothesis of past Sgr A$^\star$ flaring activity is supported by the discovery of a propagation of Fe K echoes in the Central Molecular Zone (CMZ), presumably from a source far away from the clouds (Ponti et al. 2010, 2013; Clavel et al. 2013; Ryu et al. 2013).

Fluorescent 6.4 keV emission from the GC clouds can also be provided by cosmic rays (CRs). This alternative explanation is based on the knowledge that the GC medium is filled by relatively low-energy CRs (Indriolo et al. 2010) that ionize the interstellar gas at high level, which is not observed in other parts of the Galaxy (Oka et al. 2005; Goto et al. 2008, 2011). Until recent time, the line emission from several GC clouds like the Arches cluster region, Sgr C, G0.162−0.217, G0.11−0.11 and others (see Fukuoka et al. 2009; Tatischeff et al. 2012; Yusef-Zadeh et al. 2013b) was considered as best candidates for CR ionization; however, fast variability recently observed in these clouds (Clavel et al. 2013, 2014; Terrier et al., in preparation) provided strong support for the photoionization model. Although the photon origin of the fluorescent iron line emission seems to be widely accepted, Yusef-Zadeh et al. (2013b) developed a model of the line production by non-thermal electrons (see also Yusef-Zadeh, Law & Wardle 2002; Yusef-Zadeh et al. 2007, 2013a), which could also explain to some extent the flux time variability from the GC clouds. However, Dogiel et al. (2014) argued that (i) the global distribution of relativistic electrons in the GC medium interacting with diffuse low-density gas provides a CR ionization rate that is too low to produce the observed intensity of the 6.4 keV line emission and (ii) the origin of the observed simultaneous time variations from dense molecular clouds requires many local electron sources also having simultaneous behaviours, which seems unlikely. From the other side, local sources of CRs interacting with denser gas may provide an excess of the 6.4 keV line emission in some of the GC molecular clouds, as recently demonstrated by Yusef-Zadeh et al. (2016), who found the interaction of a non-thermal source with molecular clouds in Sgr B2, traced by OH (1720 MHz) masers (see also Hollis et al. 2007; Yusef-Zadeh et al. 2013b). The general question remains: which part of the line flux from the GC molecular clouds is produced by the CRs?

Based on the archival *XMM* data of the GC region, Capelli et al. (2011b) and Tatischeff et al. (2012, hereafter T12) constructed Fe K$\alpha$ emission line maps of the Arches cluster region at 6.4 keV and showed that this emission extends well beyond the stellar cluster. Capelli et al. (2011b) argue that the observed Fe K$\alpha$ line flux and the high value of the EW suggest that the fluorescence originates from the photoionization of the cloud by X-ray photons, although excitation by CR is not specifically excluded. T12 suggested that the Fe K$\alpha$ 6.4 keV line emission observed around the Arches cluster is likely produced by bombardment of molecular gas by low-energy cosmic ray protons (LECR*p*). The authors suggest that the required large flux of low-energy CR particles could be produced in the ongoing supersonic collision between the star cluster and a nearby molecular cloud.

Using the first hard X-ray focused observation of the Arches cluster region, performed with *Nuclear Spectroscopic Telescope Array* (*NuSTAR*), we showed in our previous work (Krivonos et al. 2014, hereafter K14) that the continuum emission in the 10–20 keV band is significantly detected around the Arches cluster with a spatial morphology consistent with the Fe K$\alpha$ fluorescent line emission.

**Table 1.** List of the X-ray observations of the Arches cluster with *XMM–Newton* and *NuSTAR* used in this work.

| Mission | Date | ObsID | Exp. (ks) | Frac.[a] (per cent) |
|---|---|---|---|---|
| *XMM–Newton* | 2015-09-27 | 0762250301 | 112.0 | 78/84/60 |
| *NuSTAR* | 2015-10-19 | 40101001002 | 107.2 | 100/0 |
| *NuSTAR* | 2015-10-25 | 40101001004 | 107.8 | 100/0 |

*Note.* [a]Good time fraction for *XMM–Newton* MOS1/MOS2/PN and *NuSTAR* FPMA/FPMB, respectively. Note that *NuSTAR* FMPB data were completely rejected due to stray light contamination (Section 2.2).

Clavel et al. (2014, hereafter C14) analysed the long-term behaviour of the Arches cluster cloud (or simply the Arches cloud) over 13 yr and reported a 30 per cent decrease (4$\sigma$ confidence) in Fe K$\alpha$ line and continuum flux of the cloud emission, providing significant evidence for the X-ray reflection scenario. Despite this success, the question of determining the illuminating hard X-ray source and reflection geometry remains open. The source cannot lie within the Arches cluster, according to constraints drawn from the Fe K$\alpha$ line flux (T12) and hard X-ray continuum (K14), leaving the possibility for putative past activity of Sgr A$^\star$. In this work we track further the evolution of the flux of the Fe K$\alpha$ line with *XMM–Newton* observations and measure the shape of the hard X-ray continuum with *NuSTAR*.

Although the CR-only scenario is practically ruled out by the observed variability for most of the measured non-thermal emission, the origin of the remaining faint emission is not so obvious. As the non-thermal flux decreases, we might now be observing a significant contribution from a putative steady background level, which could be created by a different process than the one responsible for the bulk of variable emission. In this paper, we repeat the spectral fit performed by K14 to derive updated constraints for both the X-ray photoionization and the LECR emission models based on the spectral shape above 10 keV using the *NuSTAR* data taken in 2015.

The paper is structured as follows. In Section 2, we describe observations of the Arches cluster with *XMM–Newton* and *NuSTAR* in 2015 and outline the corresponding data analysis. Spectral modelling of the Arches cluster core and cloud emission is presented in Section 3. Discussion of the results obtained and the summary can be found in Sections 4 and 5, respectively. Additional materials (e.g. serendipitous detection of the Sgr A complex and a description of 2D image spectral extraction procedure) are placed in the appendix.

## 2 OBSERVATIONS AND DATA ANALYSIS

### 2.1 *XMM–Newton*

The *XMM–Newton* data reduction was carried out using the *XMM–Newton* Extended Source Analysis Software (ESAS; Snowden et al. 2008) included in version 14 of the *XMM–Newton* Science Analysis Software (SAS). We followed the procedure described by C14, using the SAS EMCHAIN and EPCHAIN scripts to produce the calibrated event lists and ESAS MOS-FILTER and PN-FILTER to exclude periods affected by soft proton flaring. Table 1 provides information about the *XMM* observations that we used.

The *XMM–Newton* source and astrophysical background spectra were extracted from these clean event lists with the ESAS MOS-SPECTRA and PN-SPECTRA tasks. For the 'Cloud' region (see below), we also extracted the corresponding quiescent particle background (QPB)

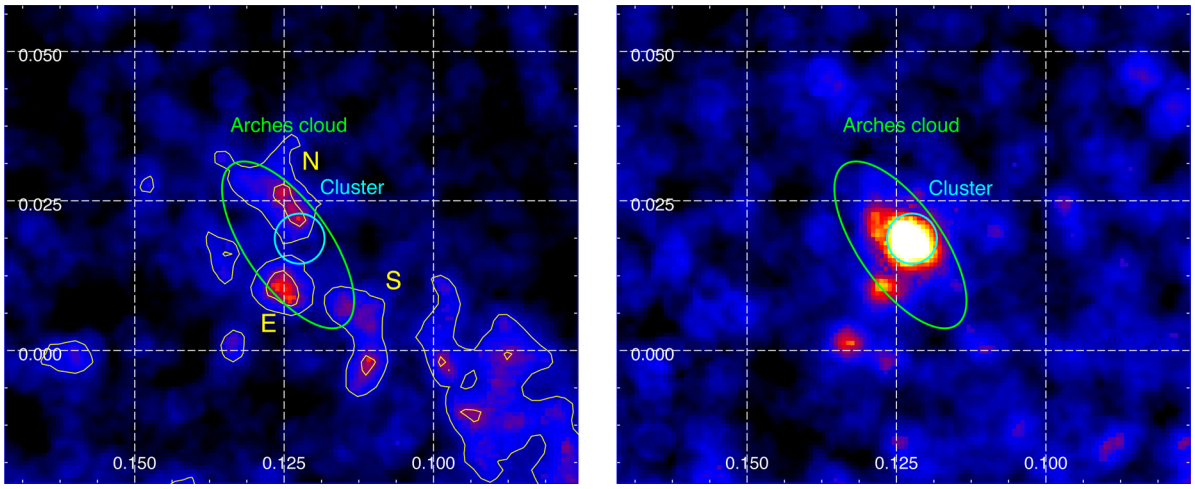


**Figure 1.** *XMM–Newton* K$\alpha$ line mosaic image of the Arches cluster region of the iron at 6.4 keV (left) and 6.7 keV (right) obtained in 6.32–6.48 and 6.62–6.78 keV energy bands, respectively. The images are continuum subtracted and adaptively smoothed. The contours in the left-hand image are shown to highlight bright clumps of 6.4 keV emission. Hereafter, the images and sky grid are shown in Galactic coordinates, with north up and east to the left, and grid spaced in degrees.

**Table 2.** Definitions of the sky regions.

| RA (J2000) | Dec. (J2000) | Parameters |
|---|---|---|
| | Cluster (circle) | |
| $17^h45^m50\overset{s}{.}3$ | $-28°49'19''$ | 15 arcsec |
| | Cloud (ellipse) | |
| $17^h45^m51\overset{s}{.}0$ | $-28°49'16''$ | 25 arcsec, 59 arcsec, 155° |
| $17^h45^m50\overset{s}{.}3$ | $-28°49'19''$ | 15 arcsec (excl.) |
| | Arches cluster complex (circle) | |
| $17^h45^m50\overset{s}{.}3$ | $-28°49'19''$ | 50 arcsec |
| | Background (annulus) | |
| $17^h45^m50\overset{s}{.}3$ | $-28°49'19''$ | 130 arcsec |
| $17^h45^m50\overset{s}{.}3$ | $-28°49'19''$ | 70 arcsec (excl.) |

*Note*. Central position and radius for circular regions, and semiminor/major axes and rotation angle for the elliptical regions. The rotation is defined counterclockwise relative to north (upward). Background region is shown in Fig. 2. 'Cluster' and 'Cloud' regions are illustrated in Fig. 1. The excluded regions are marked as 'excl.'.

from the filter wheel closed event lists provided by the ESAS calibration data base and normalized them to the level of QPB in the observations, using PN_BACK and MOS_BACK. Spectrum counts were grouped to have at least 30 counts per bin so that we can validly use $\chi^2$ statistics for fitting (Section 3).

Fig. 1 shows Fe K$\alpha$ images at 6.4 and 6.7 keV obtained, respectively, in 6.32–6.48 and 6.62–6.78 keV energy bands (see Appendix A for maps production). As expected, the stellar cluster is bright at 6.7 keV line revealing strong thermal radiation in the stellar cluster. The Arches cluster core thermal emission located within the circular region of $R \sim 15$ arcsec is embedded in the elongated non-thermal emission of the cloud with dimensions of $\sim 25 \times 59$ arcsec$^2$. In order to perform spatial and spectral analysis consistent with recent studies of the Arches cluster region (T12; C14; K14), we adopt the same sky regions to describe the core of the Arches cluster and the surrounding cloud region listed in Table 2. The cloud region is represented by an ellipse excluding the circular region of the stellar cluster.

### 2.2 *NuSTAR*

The *Nuclear Spectroscopic Telescope Array* (*NuSTAR*) hard X-ray orbital telescope (Harrison et al. 2013) provides arcminute angular resolution imaging at energies above 10 keV not accessible by any previously or currently operating missions. *NuSTAR* carries two identical co-aligned X-ray telescopes with an angular resolution of 18 arcsec (full width at half-maximum, FWHM). The focal plane detector units of each telescope, referred to as focal plane module A and B (FPMA and FPMB), cover a wide energy band 3–79 keV, and provide spectral resolution of 400 eV (FWHM) at 10 keV.

The Arches cluster was serendipitously observed during the GC region campaign (Mori et al. 2015) with the *NuSTAR* in 2012 October. Despite the fact that the Arches was observed at high off-axis angle, i.e. with low efficiency, K14 showed that the continuum 10–20 keV emission at that time was significantly detected around the Arches cluster with a spatial morphology consistent with the Fe K$\alpha$ fluorescent line emission. To better constrain the spectrum, morphology and variability of the hard X-ray non-thermal emission of the Arches cluster, we initiated the dedicated on-axis observations performed in 2015 with the total exposure of 200 ks (see Table 1).

The *NuSTAR* detectors can register X-rays passing outside the X-ray optics modules due to gaps in detector shielding (see e.g. Wik et al. 2014; Mori et al. 2015). Unfocussed flux of direct ('zero-bounce') photons or so-called 'stray light' can be a significant contributor to the detector background if there are bright X-ray sources within 2°–5° of the *NuSTAR* field of view (FOV). Examining FPMB data, we noticed strong stray light contamination from well-known X-ray burster GX 3+1 (e.g. Kuulkers 2002; den Hartog et al. 2003) covering the Arches cluster region, which led to rejection of FPMB data in the following analysis. In addition to that, FPMA data taken in 2015 were contaminated by ghost-rays ('one bounce' photons) from two nearby bright sources. The visible ghost-ray patterns are consistent with the position of persistent X-ray source 1E 1743.1−2843 (see e.g. Lotti et al. 2016, and references therein) and transient low-mass X-ray binary AX J1745.6−2901, which started its prolonged outburst in 2013 July (Degenaar et al. 2015; Ponti et al. 2015) and faded in 2016 (Degenaar et al. 2016). Nevertheless, the Arches cluster core and cloud are not strongly

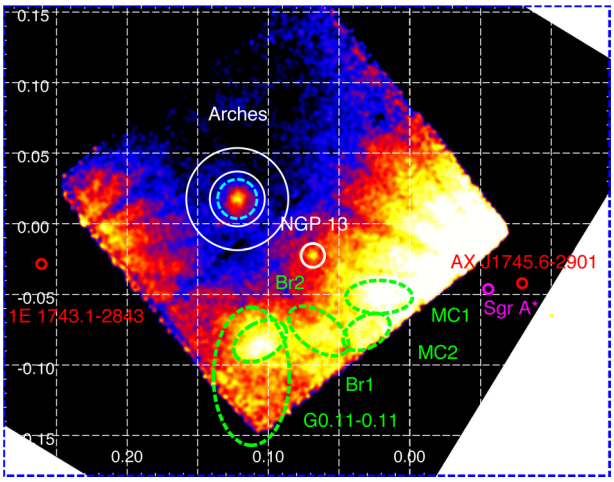


**Figure 2.** *NuSTAR* image of the Arches cluster region in 3–79 keV energy band based on FPMA data only. The image is based on two *NuSTAR* observations and comprises 215 ks of exposure time. The position of the Arches cluster is shown by the cyan circle ($R = 50$ arcsec) marked in a dashed style. The source and background spectrum are extracted, respectively, from the same cyan circle and white annulus region ($R_{\rm min} = 70$ arcsec, $R_{\rm max} = 130$ arcsec). The sources of ghost-ray contamination are shown by red labels. Green sky regions reveal positions of selected Sgr A molecular clouds (Clavel et al. 2013). The white circle with label NGP 13 denotes position of an X-ray point source from the *NuSTAR* survey of the GC region (Hong et al. 2016), also being a counterpart of the *Chandra* point source CXOUGC J174551.9−285311 (Muno et al. 2009).

contaminated and can be well localized in FPMA images as obviously seen in Fig. 2, and also based on actual ghost-rays seen in other *NuSTAR* observations (Bodaghee et al. 2014).

Note that the celestial coordinates of each photon registered with *NuSTAR* are determined with some uncertainty caused by thermal bending and external forces acting on the mast during orbit. The systematic shift of the source position can be as high as 10 arcsec. We noticed an offset of the cluster core in 2015 data at the level of ∼4 arcsec. Since the first *NuSTAR* serendipitous observation of the Arches cluster taken in 2012 demonstrated good agreement between the position of the cluster core and bright *Chandra* sources in it, we use core centroid coordinates RA $= 17^{\rm h}45^{\rm m}50\overset{\rm s}{.}52$, Dec. $= -28^\circ49'22\overset{''}{.}41$ measured in K14 as a reference position[1] to correct sky coordinates of each incoming photon in 2015 data set.

The angular separation of the Arches stellar cluster and cloud is sufficient to spatially resolve these emission components with *NuSTAR*. However, spectral analysis of the given area is seriously complicated due to the wide wings of the *NuSTAR* point spread function (PSF): the corresponding half-power diameter (enclosing half of the focused X-rays) reaches ∼60 arcsec (Madsen et al. 2015), which causes partial confusion of the Arches cluster and its cloud. Taking the above into account, we extract the spectrum of the Arches cluster from a circular region with $R = 50$ arcsec pointed at the cluster centroid position, covering both the cluster core and the cloud. The spectrum was extracted using the NUPRODUCTS task of the *NuSTAR* Data Analysis Software (NUSTARDAS) v.1.5.1 and HEASOFT v6.17. The background spectrum was extracted from the annulus region within the radii range $R = 70$–$130$ arcsec, chosen as a result of a trade-off between the representative background and ghost-ray contamination.

[1] Note that table 3 in K14 contains mistaken centroid position of the Arches cluster core, the coordinates RA $= 17^{\rm h}50^{\rm m}50\overset{\rm s}{.}43$, Dec. $= -28^\circ49'23\overset{''}{.}07$ should be read as RA $= 17^{\rm h}45^{\rm m}50\overset{\rm s}{.}52$, Dec. $= -28^\circ49'22\overset{''}{.}41$.

## 3 SPECTRAL MODELLING

In this section, we describe the details of our spectral analysis of the different regions of the Arches cluster, namely: (i) the core of the stellar cluster within $R = 15$ arcsec circular region; (ii) the cloud ellipse region and (iii) the circular area of $R = 50$ arcsec containing both cluster core and cloud, also referred later as 'the Arches cluster complex' (for the region coordinates, see Table 2). We first analyse *XMM–Newton* and *NuSTAR* data alone, comparing with previous observations and constructing the time evolution of the cloud non-thermal emission, then we present the first *XMM–Newton* and *NuSTAR* broad-band joint spectral fit of the Arches cluster complex and finally perform 2D image analysis to separate stellar cluster and cloud emission. The uncertainty estimates of the fitted model parameters in the following discussion are shown at the 90 per cent confidence level.

We begin with spectral analysis of the Arches core emission to check the consistency of its spectral shape with previous observations and to validate our data reduction procedures.

### 3.1 *XMM–Newton*: cluster emission

We extracted the spectrum of the Arches cluster from a 15-arcsec circular region and the corresponding instrumental and astrophysical background from an annulus region around the cluster (Table 2). The Arches cluster X-ray emission, which likely originates in one or more extreme colliding wind massive star binaries (Capelli et al. 2011a), is dominated by a thermal emission with prominent iron 6.7 keV line; however, at the same time, contribution from X-ray bright clouds is not negligible. We thus model the emission of the cluster region with an APEC plasma component and a non-thermal component composed by a power-law continuum and Fe 6.4 keV line. All the spectral emission components were subject to interstellar photoelectric absorption modelled with WABS in XSPEC. APEC thermal plasma model is characterized by $kT$, $Z/Z_\odot$ and $I_{kT}$ parameters, respectively, describing temperature, metallicity relative to solar and normalization in units of $10^{-18}\int n_{\rm e}n_{\rm H}\,{\rm d}V/(4\pi D^2)$, where $n_{\rm e}$ and $n_{\rm H}$ are the electron and proton number densities in units of cm$^{-3}$, and $D$ is the cluster distance in cm. Based on the previous observations of the Arches cluster with *XMM–Newton* (Wang et al. 2006; T12), we fixed the metallicity to $Z = 1.7\,{\rm Z}\odot$ throughout the paper. This model provides relatively good-fit statistics expressed by reduced $\chi^2_{\rm r} = 1.15$ for 240 degrees of freedom (d.o.f.). The best-fitting parameters of the current model are summarized in Table 3 (Model 1) and the corresponding MOS1/MOS2/PN spectra are shown in Fig. 3. Note that we also fixed the energy of the 6.4 keV line due to its low flux relative to the bright 6.7 keV line, which causes systematic shift towards higher energies.

The value of $N_{\rm H}$ is higher than the Galactic value in the direction to the Arches cluster ($N_{\rm H} = 1.2\times10^{22}$ cm$^{-2}$; Kalberla et al. 2005) by an order of magnitude, which indicates strong local absorption, most likely caused by both strong stellar winds of massive stars in the cluster and nearby molecular material of the cloud. The temperature of the thermal emission $kT = 1.82 \pm 0.10$ keV is consistent with the previous measurement (Capelli et al. 2011a; T12). The hard power-law continuum $\Gamma \sim 1$ emission is also in agreement with that found in previous studies. However, the uncertainties mainly caused by the low statistics and the soft energy range $E < 10$ keV are large.

**Table 3.** Best-fitting spectral model parameters for the Arches cluster core emission ($R = 15$ arcsec circular region) measured with *XMM–Newton*.

| Parameter | Unit | Model 1[a] | Model 2[b] |
|---|---|---|---|
| $N_{\rm H}$ | $10^{22}$ cm$^{-2}$ | $8.7 \pm 0.5$ | $11.2 \pm 1.0$ |
| $kT$ | keV | | $0.22^{+0.08}_{-0.05}$ |
| $I_{kT}$ | (see Section 3.1) | | $2^{+17}_{-2} \times 10^3$ |
| $kT$ | keV | $1.8 \pm 0.1$ | $1.58^{+0.13}_{-0.09}$ |
| $I_{kT}$ | (see Section 3.1) | $13.6 \pm 2.0$ | $23 \pm 5$ |
| $E_{6.4\,\rm keV}$ | keV | 6.4 (fixed) | 6.4 (fixed) |
| $N_{6.4\,\rm keV}$ | $10^{-7}$ photons cm$^{-2}$ s$^{-1}$ | $1.8^{+3.5}_{-1.8}$ | $1.5^{+3.6}_{-1.5}$ |
| $\Gamma$ | | $1.1 \pm 0.7$ | $0 \pm 1$ |
| $I_{\rm pow}$ | $10^{-5}$ cm$^{-2}$ s$^{-1}$ keV$^{-1}$ | $1.9^{+4.1}_{-1.4}$ | $0.3^{+1.9}_{-0.3}$ |
| $\chi^2_{\rm r}$/d.o.f. | | 1.13/240 | 1.05/238 |

*Notes.* [a]WABS × (APEC + GAUSSIAN + POWER LAW).
[b]WABS × (APEC + APEC + GAUSSIAN + POWER LAW).

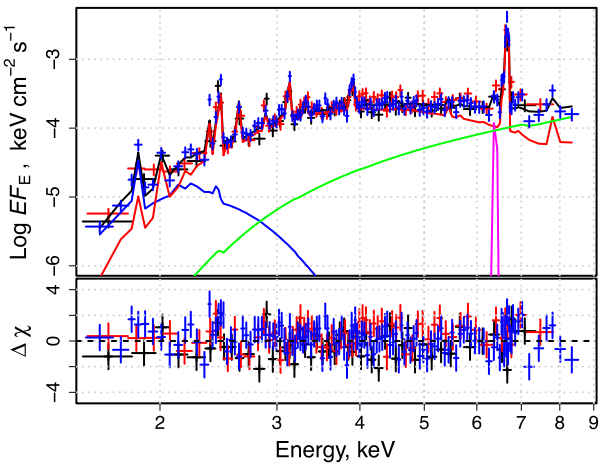


**Figure 3.** X-ray spectrum of the Arches cluster based on the long *XMM–Newton* observation performed in 2015. The spectrum was extracted from $R = 15$ arcsec circular region (Table 2). MOS1, MOS2 and PN data are shown in black, red and blue colours, respectively. The fitted model includes two APEC components with $kT = 0.22^{+0.08}_{-0.05}$ (blue) and $1.58^{+0.13}_{-0.09}$ keV (red), and non-thermal power-law continuum (green) with Gaussian 6.4 keV line coloured in magenta (Model 2 in Table 3). Hereafter, all spectra are shown in logarithmic scale, with *Y*-axis labelled with only the exponents.

Capelli et al. (2011a) reported on 70 per cent brightening of the Arches cluster emission in 2007 March/April relative to an average level of $F_{2-10\,\rm keV} = (1.5 \pm 0.1) \times 10^{-12}$ erg s$^{-1}$ cm$^{-2}$ (absorption corrected). Using the CFLUX model in XSPEC, we estimated a 2–10 keV unabsorbed total flux of the cluster of $F_{2-10\,\rm keV} = (1.5 \pm 0.3) \times 10^{-12}$ erg s$^{-1}$ cm$^{-2}$, which is fully consistent with the normal state flux level reported by Capelli et al. (2011a).

The second APEC component emission ($kT \sim 0.2$ keV), which could be due to a collection of individual stars, as suggested by T12, significantly improves the fit statistics ($\chi^2_{\rm r}$/d.o.f. = 1.05/238; Model 2 in Table 3). In contrast to T12, introducing separate absorber for the soft component of the cluster emission did not provide an improvement to the fit ($\chi^2_{\rm r}$/d.o.f. = 1.15/237, not shown in Table 3 for simplicity), which is most likely caused by the low sensitivity to the soft spectral component of our data set, based on lower exposure compared to that used by T12.

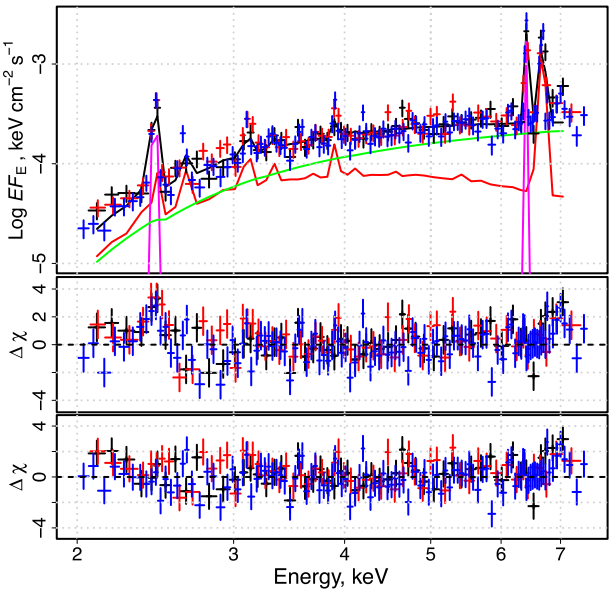


**Figure 4.** X-ray spectrum of the Arches cloud (cluster excluded) emission obtained with *XMM–Newton* MOS1 (black), MOS2 (red) and PN (blue) cameras in 2015. The model spectrum is represented by an absorbed thermal APEC component ($kT = 2.2$ keV, in red), non-thermal power-law continuum ($\Gamma = 1.6$, in green) with 6.4 keV fluorescent line emission (magenta) and K$\alpha$ line of He-like S at 2.45 keV (magenta); see Section 3.2 and Table 4 for details. Two bottom panels show residuals (data minus folded model) in terms of $\sigma$s. The middle and bottom panels demonstrate residuals of the model without and with S K$\alpha$ line included, respectively.

### 3.2 *XMM–Newton*: cloud emission

In this section we describe the spectral analysis of the cloud emission based on the data taken during the long *XMM–Newton* observation on 2015 September 27. The main question we address here is the evolution of the cloud non-thermal emission since 2012, when a drop was detected as reported by C14. Strong variation implies that a large fraction of the non-thermal emission of the cloud is due to the reflection of an X-ray transient source.

To track the evolution of the cloud emission in a way that is consistent with previous works (T12; C14), we extract *XMM–Newton* spectrum from 25 × 59 arcsec$^2$ ellipse region excluding the cluster emission (Table 2) shown in Fig. 4. Following C14, we consider the 2–7.5 keV energy range and spectral model WABS × (APEC + POWER LAW) + GAUSSIAN, fixing the temperature of the APEC plasma component to the $kT = 2.2$ keV, metallicity to $Z = 1.7\,{\rm Z}\odot$, the power-law index to $\Gamma = 1.6$ and the centroid energy and width of the Gaussian to 6.4 keV and 10 eV, respectively (C14). Because of the low statistics of the cloud region and the limited energy range selected (2–7.5 keV), the 2.2 keV APEC component represents an average temperature plasma at the position of the cloud, accounting for the soft and hard thermal diffuse emission components at 1 and 7 keV, usually considered to model the thermal background at the GC (e.g. Muno et al. 2004). For this specific analysis, we used the *XMM–Newton* instrumental background as described in C14. The best-fitting parameters of this model obtained in the 2–7.5 keV energy interval are listed in Table 4 (Model 1). The EW of the Fe 6.4 keV emission line was calculated with respect to the power-law continuum using the task EQWIDTH in SHERPA package (Freeman, Doe & Siemiginowska 2001), a part of the CIAO-4.7 software (Fruscione et al. 2006). Note that the fit with Model 1 is relatively poor ($\chi^2_{\rm r}$/d.o.f. = 1.54/224), mainly due to the strong line excess

**Table 4.** Best-fitting parameters for two models applied to *XMM–Newton* spectrum of the Arches cloud (ellipse 25 × 59 arcsec$^2$, cluster excluded). Model 1 is identical to that used in C14; Model 2 contains extra Gaussian line at 2.45 keV.

| Parameter | Unit | Model 1[a] | Model 2[b] |
|---|---|---|---|
| $N_{\rm H}$ | $10^{22}$ cm$^{-2}$ | $6.5 \pm 0.3$ | $7.1 \pm 0.4$ |
| $kT$ | keV | 2.2 (fixed) | 2.2 (fixed) |
| $I_{kT}$ | (see Section 3.1) | $4.8 \pm 0.7$ | $4.5 \pm 0.7$ |
| $E$ | keV | | $2.44 \pm 0.01$ |
| $N$ | $10^{-6}$ photons cm$^{-2}$ s$^{-1}$ | | $12 \pm 3$ |
| EW | eV | | $130 \pm 12$ |
| $E$ | keV | 6.4 (fixed) | 6.4 (fixed) |
| $N$ | $10^{-6}$ photons cm$^{-2}$ s$^{-1}$ | $3.1 \pm 0.4$ | $3.4 \pm 0.5$ |
| EW | eV | $650 \pm 60$ | $610 \pm 60$ |
| $\Gamma$ | | 1.6 (fixed) | 1.6 (fixed) |
| $N^{\rm pow}_{@\rm keV}$ | $10^{-5}$ photons keV$^{-1}$ cm$^{-2}$ s$^{-1}$ | $10.2 \pm 0.8$ | $10.8 \pm 0.9$ |
| $\chi^2_{\rm r}$/d.o.f. | | 1.54/224 | 1.21/222 |

*Notes.* [a] WABS × (APEC + POWER LAW) + GAUSSIAN.
[b] WABS × (GAUSSIAN + APEC + POWER LAW) + GAUSSIAN.

at ∼2.45 keV, presumably belonging to K$\alpha$ line from He-like sulfur (S). We first tried to add a low-temperature thermal emission component; however, this approach (i) did not remove the line at ∼2.45 keV, and hence (ii) did not improve the fit statistics and (iii) introduced the significant deviation relative to C14 method, making it difficult to compare with the long-term evolution of the cloud observed by C14. Therefore, we follow an 'ad hoc' approach described below. Because the continuum of low-temperature emission was already taken into account by an average 2.2 keV APEC plasma component, we extended the spectral model by adding a Gaussian line at ∼2.45 keV (Model 2 in Table 4). Model 2 gives a better fit ($\chi^2_{\rm r}$/d.o.f. = 1.21/222) and it does not significantly change the parameters of the non-thermal component (Table 4). This allows us to directly compare with the C14 light curve of the Arches cloud in both the 6.4 keV line emission and the power-law continuum.

The overall evolution of the normalizations of the 6.4 keV line and the reflection continuum is shown in Fig. 5, where the declining trend of the non-thermal emission of the Arches cloud is clearly seen. The 2015 *XMM–Newton* data allow us to better describe the observed trend of the Arches cloud non-thermal emission. As a zero-order approach, we model the observed flux as a constant power-law normalization parameter $N^{\rm pow}$ followed by a linear law as a function of time $N + \alpha(T - T_{\rm break})$ after sometime $T_{\rm break}$. Because of better statistics, the continuum flux is better determined from the data relative to 6.4 keV line flux. The estimated best-fitting parameters for the continuum flux evolution are listed in Table 5 and the evaluated model light curve is shown in Fig. 5 (lower panel). The corresponding decay time, when the flux decreases by a factor of 2, was estimated to be $\tau_{1/2} = 8 \pm 1$ yr. Assuming that the 6.4 keV line flux started to decline at the same time as the continuum, we run the fitting procedure with frozen $T_{\rm break}$ parameter for the Fe K$\alpha$ line flux light curve as shown in the upper panel of Fig. 5.

### 3.3 *NuSTAR*: cluster and cloud X-ray emission

In this section we describe the spectral analysis of the Arches cluster spectrum based on dedicated *NuSTAR* observations performed with the target on-axis during two 100 ks pointings in 2015 (Table 1). We check the consistency of the spectral shape of the Arches cluster with previous low-efficiency observations in 2012 when it was detected at large off-axis angles (K14). As mentioned in Section 2.2, we utilize FPMA data only, extracting the source spectrum from a circular region with a radius of 50 arcsec positioned at the centroid emission of the stellar cluster, and including the cluster and the cloud emission. The background spectrum was measured in an annular region (Table 2).

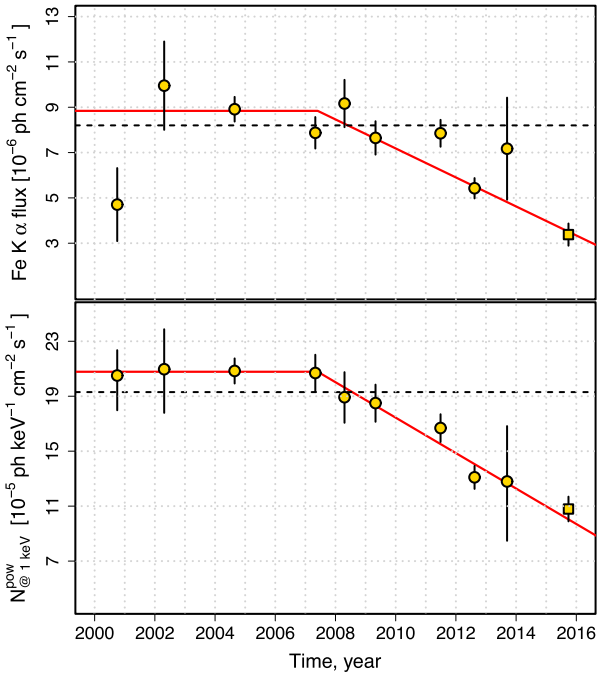


**Figure 5.** The evolution of the non-thermal emission of the Arches cloud as traced by Fe K$\alpha$ line flux (upper panel) and the reflection continuum (bottom panel) represented by a power law. The declining trend of the cloud emission reported by C14 (circle points) is confirmed by the recent measurements of the current work (square points). The dotted line represents an average emission evaluated up to 2011 by C14. The fit of the constant emission followed by a linear declining trend is shown by a dashed line.

To be consistent with K14 analysis, we utilize three spectral models, each containing a collisionally ionized plasma emission model (APEC) representing the stellar cluster thermal emission. A non-thermal emission component contains the simple power law with a Gaussian line at 6.4 keV or cosmic ray (CR)-induced emission model or a self-consistent X-ray reflection model. Although LECR-only emission model is almost excluded based on variability, we continue to test it because steady background level could be a result of CR heating, while most of the varying emission is due to reflection. All the emission components were subject to a line-of-sight photoelectric absorption model WABS in XSPEC. As the energy response of *NuSTAR* is not very sensitive for measuring the absorption column, we fixed the total absorption column at $N_{\rm H} = 9.5 \times 10^{22}$ cm$^{-2}$ measured by T12 in the core of the Arches cluster. The cross-normalization factor $C$ was introduced between the *NuSTAR* observations to validate fitting procedure. The best-fitting model parameters obtained as a result of the fitting procedure are listed in Table 6, while the *NuSTAR* spectra with model residuals are shown in Fig. 6.

This simple phenomenological model with power law provides a reliable fit to the data with $\chi^2_{\rm r}$/d.o.f. = 0.97/364. The temperature of the stellar cluster emission was not well constrained and found to have a relatively high value of $kT = 2.4^{+1.5}_{-0.4}$ keV with respect to $kT = 1.7^{+0.4}_{-0.3}$ keV measured on the *NuSTAR* data taken in 2012 with the same model (K14). The non-thermal continuum is characterized

**Table 5.** The list of the best-fitting parameters for the constant emission flux $N$ and linear law $N + \alpha(T - T_{\rm break})$ describing the evolution of the power-law non-thermal continuum and Fe K$\alpha$ flux of the Arches cloud (see Section 3.2).

| Parameter | Units | Value | |
|---|---|---|---|
| | | Power law | Fe K$\alpha$ line |
| $N^a$ | photons keV$^{-1}$ cm$^{-2}$ s$^{-1}$ | $(20.8 \pm 0.7) \times 10^{-5}$ | $(8.8 \pm 0.3) \times 10^{-6}$ |
| $\alpha$ | photons keV$^{-1}$ cm$^{-2}$ s$^{-1}$ yr$^{-1}$ | $(-1.3 \pm 0.2) \times 10^{-5}$ | $(-0.64 \pm 0.07) \times 10^{-6}$ |
| $T_{\rm break}$ | yr | $2007.4 \pm 0.5$ | 2007.4 (fixed) |

*Note.* [a]The normalization of the power law is defined at 1 keV.

**Table 6.** Best-fitting spectral model parameters for the Arches cluster $R = 50$ arcsec region emission measured with *NuSTAR*.

| Parameter | Units | Model 1[a] | Model 2[b] | Model 3[c] |
|---|---|---|---|---|
| $N_{\rm H}$ | $10^{22}$ cm$^{-2}$ | 9.5 (fixed) | 9.5 (fixed) | 9.5 (fixed) |
| $kT$ | keV | $2.40^{+1.50}_{-0.40}$ | $1.89^{+0.21}_{-0.15}$ | $1.95^{+0.32}_{-0.17}$ |
| $I_{kT}$ | (see Section 3.1) | $9.17 \pm 5.28$ | $17.46 \pm 3.50$ | $16.55 \pm 3.00$ |
| $\Delta E$ | keV | 0.1 (fixed) | | |
| $E$ | keV | $6.3 \pm 0.1$ | | |
| $F$ | $10^{-6}$ photons cm$^{-2}$ s$^{-1}$ | $3 \pm 1$ | | |
| EW | eV | $450 \pm 150$ | | |
| $\Gamma$ | | $2.4^{+0.6}_{-0.3}$ | | |
| $F^{\rm pow}_{3-20\,{\rm keV}}$ | $10^{-13}$ erg cm$^{-2}$ s$^{-1}$ | $5.6^{+1.1}_{-0.9}$ | | |
| $\Lambda$ | H-atoms cm$^{-2}$ | | $5 \times 10^{24}$ (fixed) | |
| $s$ | | | $2.3 \pm 0.4$ | |
| $E_{\rm min}$ | keV/$n$ | | $10^4$ (fixed) | |
| $N_{\rm LECR}$ | $10^{-8}$ erg cm$^{-2}$ s$^{-1}$ | | $3.2^{+1.0}_{-0.6}$ | |
| $\Gamma_{\rm RX}$ | | | | $3.3^{+\infty}_{-0.2}$ |
| $\xi$ | erg cm s$^{-1}$ | | | 10 (fixed) |
| $I_{\rm RX}$ | $10^{-5}$ | | | $7^{+1}_{-3}$ |
| $C$† | | $0.97 \pm 0.07$ | $0.96 \pm 0.07$ | $0.96 \pm 0.07$ |
| $\chi^2_{\rm r}$/d.o.f. | | 0.97/364 | 1.02/367 | 1.06/366 |

*Notes.* [a]$C \times$ WABS $\times$ (APEC + GAUSSIAN + POWER LAW).
[b]$C \times$ WABS $\times$ (APEC + LECR$p$).
[c]$C \times$ WABS $\times$ (APEC + REFLIONX).

by a steeper power law with $\Gamma = 2.4^{+0.6}_{-0.3}$ compared to $1.6 \pm 0.3$ in K14. The unabsorbed 3–20 keV flux of the continuum was estimated to be $F^{\rm pow}_{3-20\,{\rm keV}} = (0.56^{+0.12}_{-0.09}) \times 10^{-12}$ erg s$^{-1}$ cm$^{-2}$ compared to K14 measurement $F^{\rm pow}_{3-20\,{\rm keV}} = (1.5^{+0.3}_{-0.2}) \times 10^{-12}$ erg s$^{-1}$ cm$^{-2}$ in 2012. The drop of the continuum flux with a factor of $\sim$3 in 3 yr is stronger than a drop with a factor of 2 in 8 yr expected from the *XMM–Newton* data (Sections 3.2 and 3.4). The fitting procedure determines the centroid position of Fe 6.4 keV line at $E_{6.4\,{\rm keV}} = 6.3 \pm 0.1$ keV along with relatively low EW in the range 0.25–0.56 keV compared to EW $\sim$ 1 keV measured in previous works (T12; K14), confirming the lower EW measured with *XMM–Newton*. We conclude that, despite the fading of the Arches cloud emission, the non-thermal component is well constrained in 2015 observation, and still dominates the Arches cluster emission above 10 keV.

We then fitted the non-thermal emission of the cloud with the CR-induced emission model developed by T12, where the collisional ionization of the cloud by LECR$p$ reproduces the observed 6.4 keV fluorescence line strength. In contrast, the LECR electron (LECR$e$) model requires a metallicity $\gtrsim$3 times the solar value to account for the measured EW $\sim$ 1 keV, which makes the LECR$e$ model hardly compatible with the measured properties of the Arches cloud emission (T12; K14). Taking also other general arguments against the electron model given by Dogiel et al. (2014) into account, we consider only the LECR$p$ model in this work. The model depends on the proton path length in the ambient medium $\Lambda$, the minimum energy of the CR particles penetrating the cloud $E_{\rm min}$, the power-law index of the CR source energy spectrum $s$ and the model normalization $N_{\rm LECR}$ and the metallicity of the X-ray emission region $Z$. We fixed $\Lambda$ and $E_{\rm min}$ parameters of the LECR$p$ model according to T12, considering the slope $s$ and the normalization $N_{\rm LECR}$ as free parameters. The model gives an acceptable fit ($\chi^2_{\rm r}$/d.o.f. = 1.02/367). The power-law index $s = 2.3 \pm 0.4$ is generally higher than $s = 1.6^{+0.6}_{-0.5}$ measured by K14 with the *NuSTAR* data in 2012, however more consistent with $s = 1.9^{+0.5}_{-0.6}$ estimated by T12 for the LECR$p$ model with the *XMM–Newton* data. The model normalization $N_{\rm LECR} = (3.2^{+1.0}_{-0.6}) \times 10^{-8}$ erg cm$^{-2}$ s$^{-1}$ implies a power injected by LECR protons of $\sim 3 \times 10^{38}$ erg s$^{-1}$, which is a factor of $\sim$2 less than the corresponding value measured by K14. Such a decrease rules out this model as the only contribution to the non-thermal emission up to 2012.

The third model includes the self-consistent X-ray reflection model REFLIONX, which we used to describe the Arches cluster non-thermal emission in K14. REFLIONX describes the reflected spectrum for an optically thick atmosphere of constant density, illuminated by radiation with a power-law spectrum (Ross & Fabian 2005). The model predicts fluorescence lines and continuum emission. Originally developed for the surface of hot accretion discs in binary systems, REFLIONX can be well applied for cold material around the Arches cluster (K14), by fixing the ionization parameter $\xi$ at the

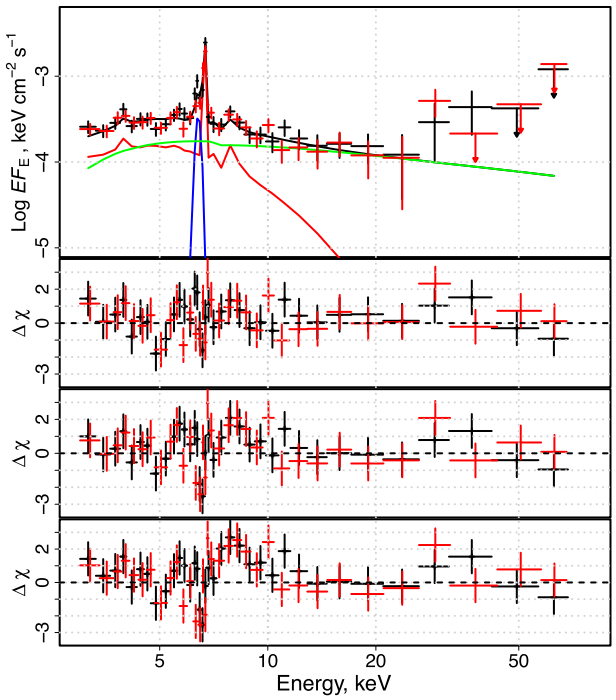


**Figure 6.** Upper panel: X-ray spectrum of the Arches cluster region as measured with FPMA during the first and second *NuSTAR* observations, shown, respectively, in red and black data points. The lines represent best-fitting spectral model (in black) with APEC (red), power law (green) and 6.4 keV Gaussian line (blue) components (Model 1 in Table 6). Given the cross-normalization factor $C$ between the observations close to unity, only one model is shown for simplicity (first observation). Bottom panels show corresponding residuals for three models listed in Table 6: power law with 6.4 keV Gaussian line, LECR$p$ and REFLIONX.

lowest allowed value of 10 erg cm s$^{-1}$. The model fits the data relatively well ($\chi^2_r$/d.o.f. = 1.06/366), with a somewhat steeper and less constrained photon index for the illuminating power-law spectrum $\Gamma_{RX} = 3.3^{+\infty}_{-0.2}$ compared to $\Gamma_{RX} = 2.9 \pm 0.3$ obtained by K14, which points to general softening of the spectrum confirmed by power-law model considered above.

We conclude that, similar to previous observations of the Arches cluster with *NuSTAR*, the 2015 spectral shape above ∼10 keV is equally well described by the X-ray photoionization and CR-induced emission models, giving no direct evidence to determine the nature of the emission mechanism. Based on this, the following joint *XMM–Newton* and *NuSTAR* spectral analysis is done only for simple power-law model.

### 3.4 *NuSTAR* and *XMM–Newton* joint fit

In the previous sections we analysed individual *XMM–Newton* and *NuSTAR* fits to check the consistency of the spectral shape of the Arches cluster with previous measurements, and we confirmed the decrease of the net flux of the non-thermal emission from the surrounding cloud in both continuum and Fe K$\alpha$ flux. Additionally, we detected a significant decrease of the EW of the 6.4 keV line, pointing to a dramatic change of the non-thermal emission of the Arches cloud, also reflected in morphology transformation. To extract more constrains on the spectral shape of the Arches cluster emission (star cluster core and extended power-law non-thermal emission together), we performed the first simultaneous *XMM–Newton*+*NuSTAR* fit on the Arches cluster complex.

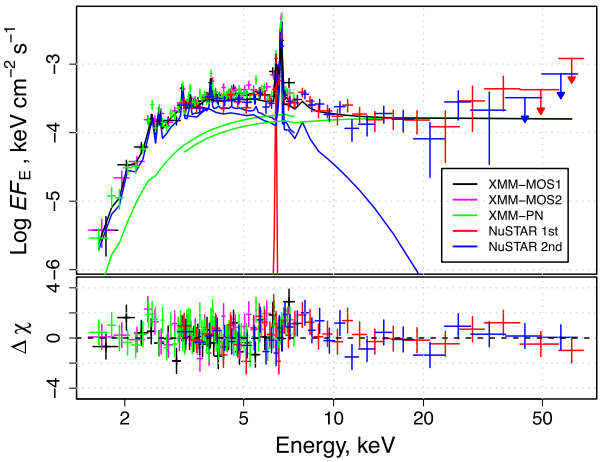


**Figure 7.** Joint *XMM–Newton* (MOS1, MOS2, PN) and *NuSTAR* (FPMA) spectrum of the Arches cluster region extracted from $R = 50$ arcsec circle shown in Fig. 2. Black line represents best-fitting model (Table 7), comprising thermal plasma (blue), fluorescent Fe K$\alpha$ 6.4 keV line emission (red) and non-thermal power-law continuum (green).

**Table 7.** Best-fitting spectral model parameters for the Arches cluster $R = 50$ arcsec region emission measured with *XMM–Newton* and *NuSTAR*. The model is described in XSPEC notation as WABS × (APEC + GAUSSIAN + POWER LAW).

| Parameter | Unit | Value |
|---|---|---|
| $N_H$ | $10^{22}$ cm$^{-2}$ | $9.3^{+0.9}_{-0.5}$ |
| $kT$ | keV | $1.95 \pm 0.14$ |
| $I_{kT}$ | (see Section 3.1) | $18 \pm 3$ |
| $E$ | keV | $6.38 \pm 0.02$ |
| $\Delta E$ | keV | 0.01 (fixed) |
| $F$ | $10^{-6}$ photons cm$^{-2}$ s$^{-1}$ | $3.1 \pm 0.6$ |
| EW | eV | $700^{+100}_{-90}$ |
| $\Gamma$ | | $2.03 \pm 0.16$ |
| $I_{pow}$ | $10^{-5}$ cm$^{-2}$ s$^{-1}$ keV$^{-1}$ | $22^{+10}_{-7}$ |
| $C$ | | $0.82 \pm 0.04$ |
| $\chi^2_r$/d.o.f. | | 1.00/918 |

Fig. 7 shows a joint *XMM–Newton* (MOS1, MOS2 and PN) and *NuSTAR* spectrum of the Arches cluster region extracted from a circular region of radius $R = 50$ arcsec around cluster's centroid, and the corresponding background spectrum for each instrument, containing the instrumental and astrophysical components, was extracted from the annular region around the Arches cluster (see Table 2 and Fig. 2). The way the source region is defined, the joint spectrum contains both thermal emission from the cluster and non-thermal emission from the surrounding cloud. To describe the data, we use the model containing, respectively, an APEC plasma model and a power-law continuum with a Gaussian line at 6.4 keV. We also added a cross-normalization constant between the *XMM–Newton* and *NuSTAR* data, fixing the former to unity. The joint spectrum is well described by the model with $\chi^2_r$/d.o.f. = 1.00/918. The model parameters are listed in Table 7. The soft thermal component is not required by the fit. The best-fitting cluster temperature was found at $kT = 1.95 \pm 0.14$ keV, which is in general agreement with *XMM–Newton* and *NuSTAR* data analysed separately in Sections 3.1 and 3.3, respectively. The cross-normalization parameter $C = 0.82 \pm 0.04$ is somewhat lower than that expected

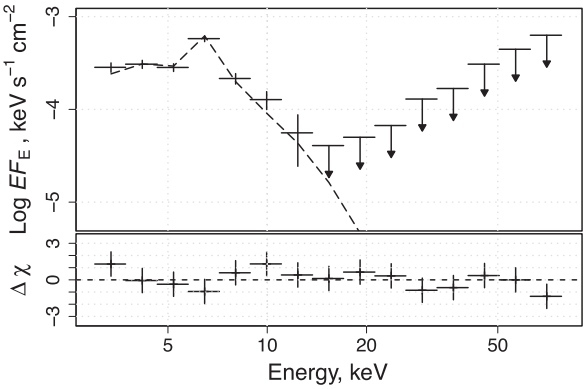


**Figure 8.** Spatially resolved *NuSTAR* spectrum of the Arches cluster core approximated with collisionally ionized plasma emission model APEC with temperature $kT = 2.4 \pm 0.4$ keV (dashed line).

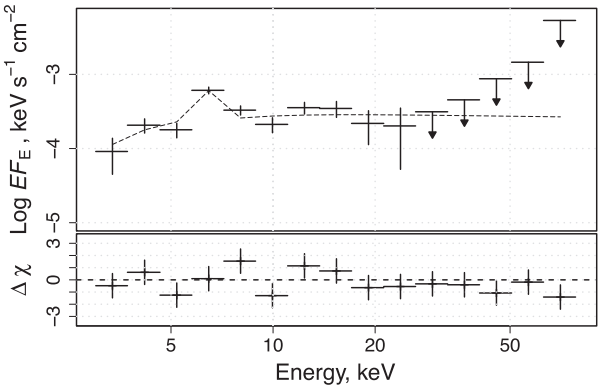


**Figure 9.** Spatially resolved *NuSTAR* spectrum of the Arches cloud modelled with power law $\Gamma = 2.1 \pm 0.3$ and 6.4 keV Gaussian line.

from relative *XMM–Newton* and *NuSTAR* cross-calibration results (Madsen et al. 2015), which is most likely caused by the overly simplified background approximation of the *NuSTAR* data, which is contaminated by ghost-rays (Fig. 2). We tested spectral extraction with different ghost-ray-free background region, and found strong deviations in the normalization of the *NuSTAR* spectrum. For instance, using the faintest possible background region, the normalization of the *NuSTAR* spectrum was a factor of ∼2 higher. However, these ghost-ray-free background regions also introduce deviations in the shape of the *NuSTAR* Arches cluster. Therefore, we conclude that the current annulus background region is the best possible solution, even if it is slightly overestimating the background contribution.

As shown from Table 7, we confirm that the $N_H$ value chosen in the *NuSTAR* spectral analysis (Table 6), and also used in K14, was valid. The joint fit gives the first solid measurement of the power law Γ up to 30–40 keV and it is consistent with other molecular clouds in the CMZ (also measured by *NuSTAR*; Mori et al. 2015; Zhang et al. 2015), pointing towards a similar origin for all clouds.

### 3.5 *NuSTAR*: spatially resolved spectrum

The Arches cluster region exhibits both thermal and non-thermal emission components originating, respectively, in the stellar cluster and nearby molecular cloud region. Despite the fact that both emission components are relatively well resolved spatially, the spectral analysis with the high resolution of *XMM–Newton* and *Chandra* still has to account for the combination of thermal and non-thermal emission components, most likely affected by projection effects. For instance, T12 model the emission of the Arches cluster region as the combination of an APEC plasma component and a non-thermal component represented by a power-law continuum and a Gaussian line at 6.4 keV.

Using the fact that thermal emission is concentrated in the stellar cluster and non-thermal cloud emission is spread more widely (i.e. these components are characterized by different spatial extent or frequency as demonstrated with the use of wavelet analysis by K14), we attempt to spatially decouple the cluster and cloud hard X-ray emission in the *NuSTAR* data in order to extract their X-ray spectra. The procedure is described in Appendix C, and the results are presented in Figs 8 and 9.

We fitted the stellar cluster emission spectrum (Fig. 8) with one APEC model subjected to a line-of-sight photoelectric absorption fixed at $N_H = 9.5 \times 10^{22}$ cm$^{-2}$. We assume that this spectrum does not include the extended non-thermal emission, so we do not need any additional components in the spectrum. This simple model provides an acceptable fit to the data with $\chi^2_r$/d.o.f. = 0.66/13. The only two free parameters were estimated from the fit: the temperature of the plasma $kT = 2.4 \pm 0.4$ keV and the unabsorbed 3–8 keV flux $(8.7 \pm 0.7) \times 10^{-13}$ erg s$^{-1}$ cm$^{-2}$. The cluster temperature is marginally higher, but it is still consistent with $kT = 1.6$–2 keV measured with *XMM–Newton* data, which is more sensitive to thermal emission (Section 3.1). In contrast, the 3–8 keV unabsorbed flux of the cluster's thermal component is somewhat lower when compared to the corresponding value of $(1.2 \pm 0.2) \times 10^{-12}$ erg s$^{-1}$ cm$^{-2}$ found with *XMM–Newton*.

Based on the 2D image spectral analysis, we assume that the spatially resolved spectrum of the Arches cloud contains the non-thermal emission only and it is not mixed with thermal radiation of the stellar cluster. The position and the width of the Gaussian line was fixed to 6.4 and 0.1 keV, respectively. The model gives acceptable fit $\chi^2_r$/d.o.f. = 1.02/12 and the power-law slope $\Gamma = 2.1 \pm 0.3$ (confirming the joint *XMM–Newton* and *NuSTAR* fit results; see Section 3.4) and the unabsorbed 3–8 and 3–20 keV fluxes to $F_{3-8\,\mathrm{keV}} = (5 \pm 1) \times 10^{-13}$ erg s$^{-1}$ cm$^{-2}$ and $F_{3-20\,\mathrm{keV}} = (9 \pm 1) \times 10^{-13}$ erg s$^{-1}$ cm$^{-2}$. The total flux of the 6.4 keV Gaussian line was estimated to be $(1.4 \pm 0.5) \times 10^{-5}$ photons cm$^{-2}$ s$^{-1}$. Given the fit statistics and uncertainties of the model parameters, we conclude that addition of cluster's thermal emission is not required.

We then applied a more physically motivated X-ray reflection model developed in the geometry of scattering X-ray incident photons from Sgr A* to the observer (Appendix D); however, we found that quality of the data does not allow us to constrain the reflection geometry.

## 4 DISCUSSION

During the long *NuSTAR* and *XMM–Newton* observations of the Arches cluster region in 2015, dedicated to monitor the emission of the molecular cloud, we observe the following distinct components in the X-ray spectra of the cluster region: an optically thin thermal plasma with a temperature $kT \sim 1.6$–2.0 keV of the stellar cluster, an additional thermal plasma component with $kT \sim 0.18$–0.20 keV of the cluster and the non-thermal emission of the cloud region characterized by a power-law continuum and fluorescent

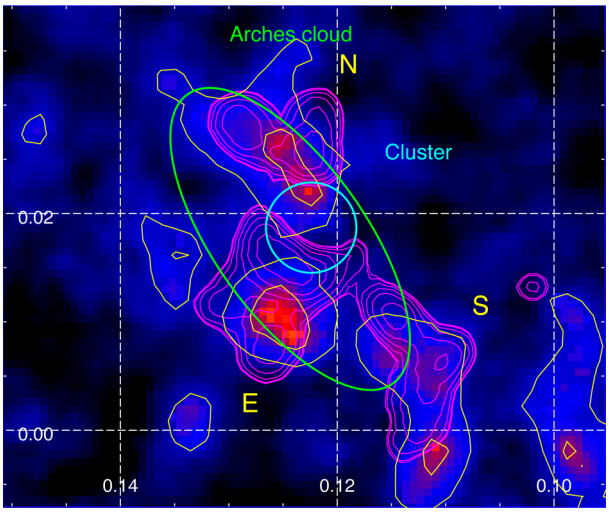


**Figure 10.** *XMM–Newton* K$\alpha$ line mosaic image of the Arches cluster region of Fe at 6.4 keV highlighted by yellow contours. Magenta contours show clumps of 6.4 keV emission based on low statistics map obtained in 2013 by C14.

Fe K$\alpha$ 6.4 keV line. In this work we present the first solid measurement of the power law $\Gamma \sim 2$ up to 30–40 keV. The *NuSTAR* spectrum extracted from a 50-arcsec region covering the cluster and the cloud region represents a mixture of the components mentioned above. Using 2D image analysis, we decoupled spectral components (Section 3.5) and confirmed the power-law slope $\Gamma$ of the non-thermal emission obtained with regular spectral analysis. The slope is consistent with that measured in other molecular clouds in the CMZ (Mori et al. 2015; Zhang et al. 2015), which points to a similar origin of non-thermal emission for all clouds. In the reflection scenario, this also means that the incident hard X-ray emission must have a power-law spectrum with $\Gamma \sim 2$ up to at least 40 keV, which adds important evidence favouring the association with past activity of Sgr A$^\star$, which exhibits a similar spectrum during X-ray flares (Barrière et al. 2014).

The morphology of the non-thermal emission of the molecular clouds near the Arches cluster reveals substructure with three bright knots to the east (E), north (N) and south (S) of the stellar cluster, marked correspondingly in Fig. 10. The current 6.4 keV line brightness distribution does not demonstrate a spatial correlation with previous morphology studies made before 2012 (Capelli et al. 2011b; T12), which showed mainly two bright spots to the north and to the south of the cluster (within the ellipse region). On the other hand, we found a similar pattern in the 6.4 keV map shown by C14 based on 2013 data set, which points towards a dramatic change of the morphology since 2012. To illustrate this, we show the current 6.4 keV map in Fig. 10 compared with contours of bright 6.4 keV clumps observed in 2013 by C14. Similar changes in morphology and appearance of new extended features are observed in other parts of the GC region (e.g. Bridge, MC1, MC2, G0.11−0.11 and Sgr B2 molecular clouds; see Appendix B and Ponti et al. 2010; Clavel et al. 2013). For instance, Zhang et al. (2015) revealed the substructure of the fading Sgr B2 cloud, with two compact cores, Sgr B2(M) and Sgr B2(N), and newly emerging cloud G0.66−0.13, which highlights that the illuminating front(s) propagating within this region has already started to leave its main cores. The similarities between the Arches cloud and the other molecular clouds also favour a similar reflection mechanism as the origin of their non-thermal emission. We confirm the variability seen by *XMM–Newton* and measure for the first time, variability of the non-thermal emission of the Arches cloud with *NuSTAR*, providing additional evidence that continuum emission above 10 keV is linked to the 6.4 keV line flux, which was not known a priori in this complex region. Strong variations of the molecular clouds in the GC support the X-ray reflection mechanism of fluorescence observed in CMZ and reveal propagation of illuminating fronts, presumably induced by the past flaring activity of Sgr A$^\star$.

The similarity with other molecular clouds is also confirmed by the long-term variability of the non-thermal emission of the Arches cloud. The fluorescent Fe K$\alpha$ emission and the hard X-ray continuum continue to demonstrate synchronous fast time variability, showing that most of the power-law continuum is coupled to the 6.4 keV line emission on a long time-scale (however, recent change of the EW in 2015 points towards an ongoing decoupling; see below). Thanks to the new observations with *XMM–Newton*, we are able to better describe the declining trend of the cloud emission. The linear fit of the varying flux, in both Fe K$\alpha$ line and hard X-ray continuum, gives a half-time decay $\tau_{1/2} = 8 \pm 1$ yr, with the emission starting to decrease in $T_{\rm break} = 2007.4 \pm 0.5$. Such strong variations have been observed not only in several other molecular clouds in the Sgr A complex (MC1, MC2 and G0.11−0.11; see Capelli et al. 2012; Clavel et al. 2013), but also in the giant molecular cloud Sgr B2 (Terrier et al. 2010), which started to fade in 2001 (Inui et al. 2009) after a decade of possibly constant emission (Revnivtsev et al. 2004). However, we should note that this tentative comparison should be used with a caution: the declining trends for both the Sgr B2 region and the Arches cloud region are averaged over relatively large regions, which could include substructures that may vary differently (Zhang et al. 2015).

C14 showed that the EW of the Fe K$\alpha$ line is compatible with being constant over time with an average value EW $= 0.9 \pm 0.1$ keV observed since 2000 (also consistent with other studies; Capelli et al. 2011b; T12; K14), indicating, similar to flux evolution, that most of the power-law continuum was linked to the 6.4 keV emission. Our analysis of the *XMM–Newton* and *NuSTAR* data of the Arches cloud region demonstrates a significant drop of the EW of the Fe K$\alpha$ 6.4 keV line to 0.6–0.7 keV. The EW decrease indicates ongoing decoupling of the iron line emission from the continuum, which may be related to a relative increase of the LECR*p* contribution (which is known to produce a lower EW). Indeed, while the absolute contribution of LECR*p* is expected to be constant over time, its relative contribution to the total amount of non-thermal emission should be increasing as the reflection component is decreasing. However, the drop in EW could also be due to a change in the geometry of the reflector. Because of the dramatic recent changes in the morphology of the 6.4 keV emission, this second explanation (or a combination of the two) should not be excluded.

In the X-ray reflection scenario, within a single cloud, the EW is only expected to increase with time (based on absorption; see e.g. Odaka et al. 2011), so a lower EW would mean that we are seeing a structure that is at a different position along the line of sight. The clumps of 6.4 keV line emission, visible in 2015 (and 2013), were not seen to be bright in 2000–2012, which means that reflection is still contributing to a certain extent to the faint 2015 emission and that the illuminating front is now reaching different clumps. If these new clumps are within the same cloud, this means that the illuminating event is rather short (the light curve average over the 'cloud' region is hiding faster variations) and if they are not part of the cloud, they are likely to be in a very different location along the line of sight and be illuminated by a different event.

## 5 SUMMARY

Recent *NuSTAR* and *XMM–Newton* observations of the molecular cloud around the Arches cluster demonstrate a dramatic change in both morphology and intensity of the non-thermal emission. Below we summarize the main results of this work.

(i) Despite the observed fading, the non-thermal continuum emission of the cloud is detected up to ∼30–40 keV. The continuum is well approximated by a power law with $\Gamma \sim 2$, which is the first direct measurement of the Arches hard X-ray continuum, consistent with other molecular clouds measured with *NuSTAR* (Mori et al. 2015; Zhang et al. 2015).

(ii) The relatively homogeneous morphology of the non-thermal emission traced by fluorescent Fe K$\alpha$ line has changed since 2012, revealing three bright clumps around the Arches cluster, which are detected in 2015.

(iii) With long *XMM–Newton* observations in 2015, we confirmed the declining trend of the non-thermal emission of the cloud reported by C14.

(iv) By fitting a simple broken linear trend to the Arches cloud emission, we showed that the constant emission of the cloud started to decline in 2007. The fading rate is consistent in both power-law continuum and 6.4 keV line flux, which indicates that most of the non-thermal continuum was linked to the fluorescent Fe K$\alpha$ 6.4 keV line emission on a long time-scale. The estimated half-life time decay, $\tau_{1/2} = 8 \pm 1$ yr, is similar to that observed in several other molecular clouds in the GC, including the giant molecular cloud Sgr B2, which adds more evidence that the same reflection mechanism is operating in both these clouds and that the main illuminating front(s) has already started to leave these clouds.

(v) We have obtained the non-thermal X-ray spectrum of the Arches cloud by carefully separating the signal from thermal emission of the cluster core. The spectrum is well described by a power-law continuum with $\Gamma \sim 2$ and a Gaussian line at 6.4 keV. A more physically motivated model based on Monte Carlo simulations fits the spectrum equally well; however, limited statistics do not allow us to constrain the reflection geometry (Appendix D).

(vi) The EW of the fluorescent Fe K$\alpha$ line revealed a sharp decrease to 0.6–0.7 keV in 2015, compared to $0.9 \pm 0.1$ keV observed over 13 yr since 2002. This could indicate a change in reflection to a different line of sight of the clumps or that the CR component has become more dominant.

(vii) The measured 2–10 keV unabsorbed total flux of the Arches cluster, $1.5 \pm 0.3 \times 10^{-12}$ erg s$^{-1}$ cm$^{-2}$, is fully consistent with its normal state flux level observed by Capelli et al. (2011a), and no outburst from the cluster was detected during our observation in 2015.

(viii) Using *XMM–Newton* and *NuSTAR* observations in 2015, we demonstrate (see Appendix B) a strong correlation between the 6.4 keV line flux and the hard 10–20 keV X-ray continuum emission of the Br1 and Br2 clouds of the 'Bridge' region (Ponti et al. 2010). The emission of MC2 cloud is dim, which confirms the decreasing trend reported in earlier works (Capelli et al. 2012; Clavel et al. 2013).

## ACKNOWLEDGEMENTS

This work has made use of data from the *NuSTAR* mission, a project led by the California Institute of Technology, managed by the Jet Propulsion Laboratory and funded by the National Aeronautics and Space Administration, and re-observations obtained with *XMM–Newton*, an ESA science mission with instruments and contributions directly funded by ESA Member States and NASA. The research has made use of the *NuSTAR* Data Analysis Software (NUSTARDAS) jointly developed by the ASI Science Data Center (ASDC, Italy) and the California Institute of Technology (USA). RK acknowledges support from the Russian Basic Research Foundation (grant 16-02-00294), the Program of the President of the Russian Federation for support of leading scientific schools (project NSh- 10222.2016.2), the Basic Research Program P-7 of the Presidium of the Russian Academy of Science, the Academy of Finland (grant 300005) and hospitality of the Tuorla Observatory, and thanks Eugene Churazov for the Monte Carlo X-ray reflection model used in the paper. GP acknowledges support by the Bundesministerium für Wirtschaft und Technologie/Deutsches Zentrum für Luft- und Raumfahrt (BMWI/DLR, FKZ 50 OR 1408 and FKZ 50 OR 1604) and the Max Planck Society. The authors would like to thank the referee for valuable comments that helped to improve the paper.

## REFERENCES

Ajello M. et al., 2016, ApJ, 826, 76
Barrière N. M. et al., 2014, ApJ, 786, 46
Bodaghee A. et al., 2014, ApJ, 791, 68
Capelli R., Warwick R. S., Cappelluti N., Gillessen S., Predehl P., Porquet D., Czesla S., 2011a, A&A, 525, L2
Capelli R., Warwick R. S., Porquet D., Gillessen S., Predehl P., 2011b, A&A, 530, A38
Capelli R., Warwick R. S., Porquet D., Gillessen S., Predehl P., 2012, A&A, 545, A35
Churazov E. et al., 1993, ApJ, 407, 752
Churazov E., Sazonov S., Sunyaev R., Revnivtsev M., 2008, MNRAS, 385, 719
Churazov E., Khabibullin I., Sunyaev R., Ponti G., 2017, MNRAS, 465, 45
Clavel M., Terrier R., Goldwurm A., Morris M. R., Ponti G., Soldi S., Trap G., 2013, A&A, 558, A32
Clavel M., Soldi S., Terrier R., Tatischeff V., Maurin G., Ponti G., Goldwurm A., Decourchelle A., 2014, MNRAS, 443, L129 (C14)
Degenaar N., Wijnands R., Miller J. M., Reynolds M. T., Kennea J., Gehrels N., 2015, J. High Energy Astrophys., 7, 137
Degenaar N., Reynolds M. T., Wijnands R., Miller J. M., Kennea J. A., Ponti G., Haggard D., Gehrels N., 2016, Astron. Telegram, 9196
den Hartog P. R. et al., 2003, A&A, 400, 633
Dogiel V. A., Chernyshov D. O., Kiselev A. M., Cheng K.-S., 2014, Astropart. Phys., 54, 33
Figer D. F., Kim S. S., Morris M., Serabyn E., Rich R. M., McLean I. S., 1999, ApJ, 525, 750
Figer D. F. et al., 2002, ApJ, 581, 258
Freeman P., Doe S., Siemiginowska A., 2001, in Starck J.-L., Murtagh F. D., eds, Proc. SPIEVol. 4477, Astronomical Data Analysis. SPIE, Bellingham, p. 76
Fruscione A. et al., 2006, Proc. SPIE, 6270, 62701
Fukuoka R., Koyama K., Ryu S. G., Tsuru T. G., 2009, PASJ, 61, 593
Goto M. et al., 2008, ApJ, 688, 306
Goto M., Usuda T., Geballe T. R., Indriolo N., McCall B. J., Henning T., Oka T., 2011, PASJ, 63, L13
Harrison F. A. et al., 2013, ApJ, 770, 103
Hollis J. M., Jewell P. R., Remijan A. J., Lovas F. J., 2007, ApJ, 660, L125
Hong J. et al., 2016, ApJ, 825, 132
Indriolo N., Blake G. A., Goto M., Usuda T., Oka T., Geballe T. R., Fields B. D., McCall B. J., 2010, ApJ, 724, 1357
Inui T., Koyama K., Matsumoto H., Tsuru T. G., 2009, PASJ, 61, S241
Kalberla P. M. W., Burton W. B., Hartmann D., Arnal E. M., Bajaja E., Morras R., Pöppel W. G. L., 2005, A&A, 440, 775
Koyama K., Maeda Y., Sonobe T., Takeshima T., Tanaka Y., Yamauchi S., 1996, PASJ, 48, 249
Krivonos R., Sazonov S., 2016, MNRAS, 463, 756
Krivonos R. A. et al., 2014, ApJ, 781, 107 (K14)

Kuulkers E., 2002, A&A, 383, L5
Lotti S. et al., 2016, ApJ, 822, 57
Madsen K. K. et al., 2015, ApJS, 220, 8
Markevitch M., Sunyaev R. A., Pavlinsky M., 1993, Nature, 364, 40
Mori K. et al., 2015, ApJ, 814, 94
Muno M. P. et al., 2004, ApJ, 613, 1179
Muno M. P. et al., 2009, ApJS, 181, 110
Murakami H., Koyama K., Sakano M., Tsujimoto M., Maeda Y., 2000, ApJ, 534, 283
Nowak M. A. et al., 2012, ApJ, 759, 95
Odaka H., Aharonian F., Watanabe S., Tanaka Y., Khangulyan D., Takahashi T., 2011, ApJ, 740, 103
Oka T., Geballe T. R., Goto M., Usuda T., McCall B. J., 2005, ApJ, 632, 882
Ponti G., Terrier R., Goldwurm A., Belanger G., Trap G., 2010, ApJ, 714, 732
Ponti G., Morris M. R., Terrier R., Goldwurm A., 2013, in Torres D. F., Reimer O., eds, Astrophys. Space Sci. Proc. Vol. 34, Cosmic Rays in Star-Forming Environments. Springer-Verlag, Berlin, p. 331
Ponti G. et al., 2015, MNRAS, 446, 1536
Porquet D., Predehl P., Aschenbach B., Grosso N., Goldwurm A., Goldoni P., Warwick R. S., Decourchelle A., 2003, A&A, 407, L17
Porquet D. et al., 2008, A&A, 488, 549
Revnivtsev M. G. et al., 2004, A&A, 425, L49
Ross R. R., Fabian A. C., 2005, MNRAS, 358, 211
Ryu S. G., Nobukawa M., Nakashima S., Tsuru T. G., Koyama K., Uchiyama H., 2013, PASJ, 65, 33
Snowden S. L., Mushotzky R. F., Kuntz K. D., Davis D. S., 2008, A&A, 478, 615
Sunyaev R., Churazov E., 1998, MNRAS, 297, 1279
Sunyaev R. A., Markevitch M., Pavlinsky M., 1993, ApJ, 407, 606
Tatischeff V., Decourchelle A., Maurin G., 2012, A&A, 546, A88 (T12)
Terrier R. et al., 2010, ApJ, 719, 143
Tsujimoto M., Hyodo Y., Koyama K., 2007, PASJ, 59, 229
Walls M., Chernyakova M., Terrier R., Goldwurm A., 2016, MNRAS, 463, 2893
Wang Q. D., Dong H., Lang C., 2006, MNRAS, 371, 38
Wik D. R. et al., 2014, ApJ, 792, 48
Yusef-Zadeh F., Law C., Wardle M., 2002, ApJ, 568, L121
Yusef-Zadeh F., Nord M., Wardle M., Law C., Lang C., Lazio T. J. W., 2003, ApJ, 590, L103
Yusef-Zadeh F., Muno M., Wardle M., Lis D. C., 2007, ApJ, 656, 847
Yusef-Zadeh F., Wardle M., Lis D., Viti S., Brogan C., Chambers E., Pound M., Rickert M., 2013a, J. Phys. Chem. A, 117, 9404
Yusef-Zadeh F. et al., 2013b, ApJ, 762, 33
Yusef-Zadeh F., Cotton W., Wardle M., Intema H., 2016, ApJ, 819, L35
Zhang S. et al., 2015, ApJ, 815, 132

## APPENDIX A: *XMM–NEWTON* CONTINUUM-SUBTRACTED IMAGES

To produce *XMM–Newton* continuum-subtracted images at 6.4 and 6.7 keV, we followed the optimized procedure presented by Terrier et al. (in preparation), which can be summarized as follows. For each instrument we produced the count, background and exposure maps with initial resolution of 2.5 arcsec, using (SAS) tasks MOS-SPECTRA, PN-SPECTRA, MOS_BACK and PN_BACK in three energy bands: 4.7–6.3, 6.32–6.48 and 6.62–6.78 keV. To estimate the continuum underlying the emission lines, we assumed the following spectral model: a power law of photon index $\Gamma = 2$ plus a thermal plasma of temperature $kT = 6.5$ keV (with abundance equal to solar), both components being absorbed by a column density $N_{\rm H} = 7 \times 10^{22}$ cm$^{-2}$. For each pixel, the normalizations of these two components were derived using the continuum emission within 4.7–6.3 keV and the line+continuum emission at 6.7 keV, allowing to subtract both the continuum emission underlying the 6.4 keV line and the non-thermal emission underlying the 6.7 keV line. After taking into account the different efficiencies of the three European Photon Imaging Camera (EPIC) detectors, the individual instrument maps were then combined to create the corresponding continuum-subtracted flux maps.

## APPENDIX B: SERENDIPITOUS DETECTION OF THE Sgr A COMPLEX

Fig. B1 shows a part of CMZ region covered by *XMM–Newton* and *NuSTAR* observations of the Arches cluster, which allows us to capture the present state of the cloud's surface brightness distribution in 2015. The cloud designation is taken from Clavel et al. (2013), who analysed the *Chandra* data of the Sgr A complex, in particular the 'Bridge' region (Ponti et al. 2010), splitting it into the two clouds Br1 and Br2, which are the brightest features in our observations. Fig. B1 demonstrates the presence of a strong correlation between the 6.4 keV line flux (*XMM–Newton*) and hard 10–20 keV X-ray continuum emission (*NuSTAR*) of Br1 and Br2. Unfortunately the region around the MC1 cloud is strongly contaminated by ghost-rays (Fig. 2). Only partly covered by the *NuSTAR* FOV, the emission of the MC2 cloud is dim, in both 6.4 keV line and hard X-ray

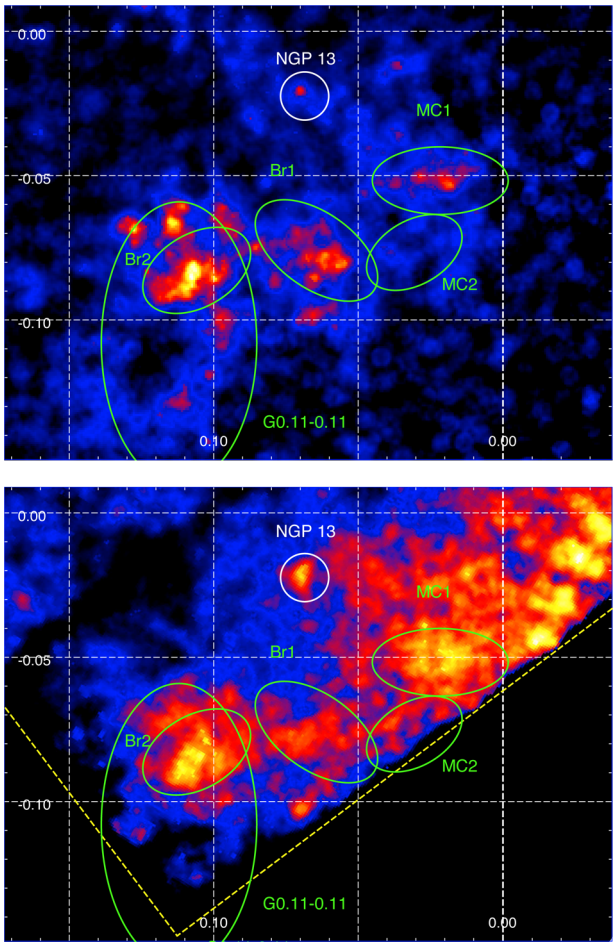


**Figure B1.** Upper panel: *XMM–Newton* image of the molecular zone complex region at 6.4 keV. Lower panel: *NuSTAR* image of the same sky region in 10–20 keV energy band. Green regions demonstrate the spatial extent of known illuminated clouds (Clavel et al. 2013) and white circle shows the position of hard X-ray point source NGP 13 (Hong et al. 2016). Yellow dashed lines delimit edges of the *NuSTAR* image.

continuum, which is in agreement with the decreasing trend reported in earlier works (Capelli et al. 2012; Clavel et al. 2013). The detailed study of the Sgr A complex based on the current *XMM–Newton* and *NuSTAR* observations will be presented in a separate paper.

## APPENDIX C: X-RAY SPECTRUM EXTRACTION FROM A 2D IMAGE

In the following procedure we repeat a similar 2D image analysis as done by Krivonos & Sazonov (2016), who analysed *NuSTAR* data of the local Seyfert 2 galaxy NGC 5643 and successfully decoupled partially confused spectra of the nucleus and an ultraluminous source located in the same galaxy.

We first combined the FPMA data from both *NuSTAR* observations into sky mosaics in 15 energy bands logarithmically covering the *NuSTAR* working energy range 3–79 keV. Each sky image was analysed with the SHERPA package. The spatial model of the Arches cluster includes two 2D Gaussians. The first represents the stellar cluster emission, with the position fixed at the core centroid coordinates measured in K14 (see Section 2.2) and width fixed at 4 arcsec FWHM (PSF smearing effect). Similar to that, the second Gaussian was aligned with the corresponding 'halo' Gaussian component used in K14 to describe the cloud emission, setting the position at RA $= 17^{h}45^{m}50\overset{s}{.}62$, Dec. $= -28^{\circ}49'47\overset{''}{.}17$ and FWHM model parameter at 72.4 arcsec. Despite the fact that the morphology of the cloud emission has been changed since 2012, the 'halo' Gaussian still covers the spatial extent of the molecular cloud region. The amplitudes of the 2D Gaussians were free parameters. The background term was estimated in the annulus $70 < R < 130$ arcsec shown in Fig. 2. By running the fitting procedure in each of the 15 energy bands, we extracted the detector Pulse Height Amplitude (PHA) spectrum of both spatial components. The corresponding Redistribution Matrix File (RMF), which maps from energy space into PHA space, was simply adopted from standard spectral analysis with NUPRODUCTS (Section 2.2) and rebinned with RBNRMF tool of HEASOFT 6.19 package. Following the approach described in Krivonos & Sazonov (2016), we calibrated Auxiliary Response File (ARF), utilizing the *NuSTAR* data of a bright source with a known spectrum. To this end we used a 20-ks observation (ObsID: 80001003002) of the MeV blazar PMN J0641−0320 with a very hard power-law spectrum of $\Gamma \approx 1$ detectable up to ∼80 keV (Ajello et al. 2016). Here we assume that the ARF calibrated for a point-like source is suitable for the extended emission of the Arches cloud. Given the limited statistics of the *NuSTAR* Arches cluster observations, the deviations are within the uncertainties.

Spatially decoupled spectra of the Arches cluster core and extended cloud emission are shown in Fig. C1. X-ray emission of the cluster contains an excess in the 5.8–7.2 keV range, compatible with ∼6.7 keV line and rapidly drops above ∼10 keV as expected for thermal emission with $kT \approx 2$ keV. Non-thermal emission of the extended cloud component apparently includes excess around 6.4 keV and dominates above 10 keV. This is consistent with what was inferred from the *NuSTAR* images in the 3–10, 6–7 and 10–20 keV energy bands (K14).

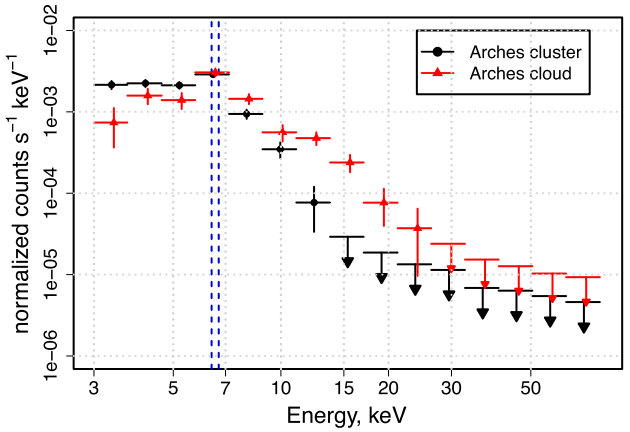


**Figure C1.** Spatially resolved *NuSTAR* spectra of the Arches cluster core (black) and cloud (red) X-ray emission. The position of Fe K$\alpha$ 6.4 and 6.7 keV is marked by vertical dashed lines, as in the *NuSTAR* standard spectra these two lines cannot be separated by our technique. The upper limits are $1\sigma$ errors.

## APPENDIX D: X-RAY REFLECTION MODEL

The X-ray reflection model, based on Monte Carlo simulations of the radiative transfer in the gas cloud, was initially developed for calculation of an X-ray albedo of the Earth atmosphere (Churazov et al. 2008). The model was later modified to the geometry more appropriate for illumination of GC molecular clouds. Namely, a uniform spherical cloud is illuminated by an external source with a given spectrum (Churazov et al. 2017). The spectrum emerging from the molecular cloud depends on several parameters: the slope ($\Gamma$) of the incident power-law spectrum, the cloud optical depth to Thomson scattering $\tau_T = \sigma_T(2n_{H_2})r$, where $n_{H_2}$ is the number density of hydrogen molecules and $r$ is the cloud radius, the iron abundance relative to solar, the scattering angle ($\theta$) for photons

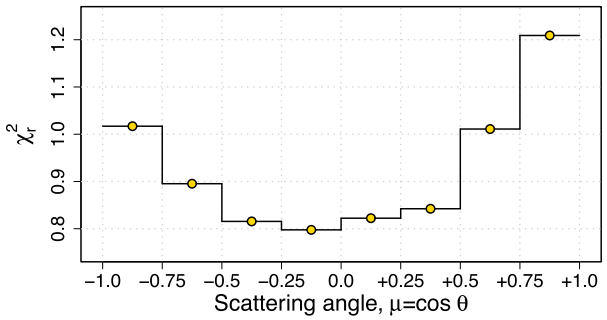


**Figure D1.** Reduced $\chi^2$ fit statistics for 14 d.o.f. of the Arches cloud *NuSTAR* spectrum fitted with the X-ray reflection model as a function of the scattering angle $\theta$.

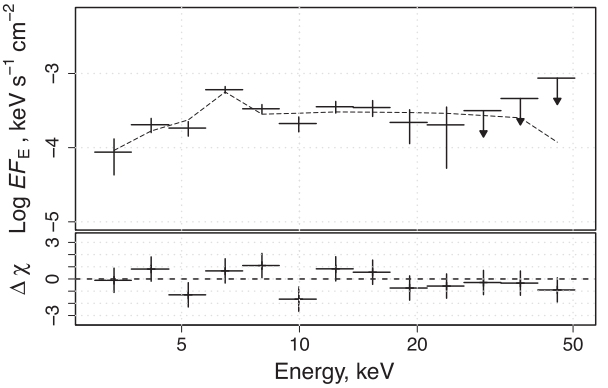


**Figure D2.** Spatially resolved *NuSTAR* spectrum of the Arches cloud modelled with X-ray reflection model.

travelling from Sgr A$^\star$ to the Arches cloud and then to the observer and the interstellar medium (ISM) line-of-sight column density towards the cloud ($N_{\rm H}$).

In the current model set-up we fixed the power-law slope of the incident Sgr A$^\star$ spectrum at $\Gamma = 2$, consistent with what was measured above, Sgr B2 X-ray reflection scenarios (Revnivtsev et al. 2004; Terrier et al. 2010; Zhang et al. 2015; Walls et al. 2016), and observed for Sgr A$^\star$ flares (Porquet et al. 2003, 2008; Nowak et al. 2012; Barrière et al. 2014). The optical depth of the cloud was not constrained by the fit ($\tau_{\rm T} < 0.06$), and was fixed at the lowest value allowed by the model $\tau_{\rm T} = 0.02$, which is in turn consistent with Capelli et al. (2011b) measurements $\tau_{\rm T} = 0.01$–$0.03$ of the north and south bright Fe K$\alpha$ knots of the Arches cloud. The metallicity was fixed to $Z = 1.7\,{\rm Z}_\odot$, in accordance with the whole analysis of this paper. To cover a wide range of scattering angles $\theta$ from 180° (backscattering) to 0°, we built a set of eight models for different $\mu = \cos(\theta)$, ranging from –1.0 to 1.0 with step of 0.25. Fig. D1 shows fit statistics for the models as a function of $\mu$. As seen from the figure, the quality of the data formally allows a wide range of the scattering angles $\theta$, however revealing local extremum at $\mu = -0.25$–$0.0$ ($\theta = 90^\circ$–$105^\circ$), suggesting that the cloud be located at or slightly further away the Sgr A$^\star$ distance. The corresponding spectral fit is shown in Fig. D2.

This paper has been typeset from a TEX/LATEX file prepared by the author.